Magazine of Civil Engineering

ISSN 2712-8172

journal homepage: http://engstroy.spbstu.ru/

Research article

UDC 621.5

DOI: 10.34910/MCE.112.12

Flexural behavior of 60 m UHPC pre-stressed box girder

V.T. Nguyen[a], ***V.C. Mai***[b]*

[a] *Le Quy Don Technical University, Ha Noi, Viet Nam*

[b] *Kumoh National Institute of Technology, Gumi, Gyeongbuk, South Korea*

maivietchinh@lqdtu.edu.vn

Keywords: concrete damage plasticity, simulation model, box girder, four-point bending, ultra high performance concrete

Abstract. In recent years, an emerging technology of Ultra High Performance Concrete (UHPC) has become popular in the construction industry and has been applied in many countries around the world. However, this material technology is still relatively new in Vietnam. The present investigation is a study on enhancement in flexural performance and the effectiveness of UHPC box girder strengthened with pre-stressed tendons, which was adapted from the first project of a high-speed train in Vietnam. A 3D simulation model of a 60 m UHPC pre-stressed box girder was implemented using concrete damage plasticity (CDP) approach. The validity of the proposed model is ensured by comparing the simulation results with experimental data. The parametric studies were then performed using the validated finite element model to analyze the flexural behavior of the 60m UHPC pre-stressed box girder. It was concluded that the developed models can accurately capture the behavior and predicts the load-carrying capacity of the UHPC girder. The present research contributes to the development and application of advanced UHPC concrete technology in Vietnam as well as emphasizes effective designs that significantly reduce self-weight and enhance loading capacity for super long-span girders.

Citation: Nguyen, V.T., Mai, V.C. Flexural behavior of 60 m UHPC pre-stressed box girder. Magazine of Civil Engineering. 2022. 112(4). Article No. 11212. DOI: 10.34910/MCE.112.12

1. Introduction

The population explosion in the big cities around the world leads to a rapid increase in the continuous development of transportation infrastructure. And, in this particular scenario, utilizing the full capacity of the material, decreasing the self-weight, increasing the efficiency of the bearing structure, and finally optimizing construction cost, particularly, for a super long span of the structural girder, become the important tasks for structural engineers and researchers. Ultra high performance concrete (UHPC) is an advanced concrete material with superior property both in mechanical and chemical properties is the potential choice to fulfill demanding design requirements. Due to its high packing density with a very low water-to-binder ratio (w/b) and the addition of reactive mineral powder [1–3], such as silica fume, compared with normal concrete, UHPC possesses many superior properties, such as high flowability, high strength, abrasion and impact resistance, low permeability and high durability [4–11]. UHPC offers new opportunities for infrastructure works, building constructions, particularly for super long-span structures. UHPC is considered as an advanced material for the future [12] and is intensively researched in many developed countries including USA [13], Germany [14], France [15, 16], Netherlands [17], Canada [18], Austria [19], Australia [20], New Zealand [21], Republic of Korea [22, 23], and Japan [24]. According to collected data, Y.L. Voo revealed more than 200 bridges are using UHPC as the main bearing structure or the supported parts [25].

The experimental studies of flexural behavior of pre-stressed UHPC girder were implemented by Min-Seon Jeong et al [26] for segmental box girders, by Lee Seung-Jae et al [27] for UHPC pre-stressed

T-beams, by Qing-Young Guo et al [28] for segmental box shaped girders. However, abovementioned studies contribute to field of short-span UHPC girders, more studies are needed for large-scale structures. In the simulation aspect, Luaay Hussein investigated flexural behavior on three series of UHPC-NSC/HSC composite girders by simulation model in Abaqus. The proposed model was validated by experimental results. The comparison between the FE model and test for UHPC-NSC/HSC composite girder showed very close results [29]. M. Singh et al implemented experimental and numerical investigations of a 3.5 m UHPC girder. Numerical simulation was analyzed in Abaqus. The ultimate load capacity predicted by the FEM model is 4 % disparity compared to the test's result [30]. By the numerical simulation in Abaqus, Chen and Graybeal studied three different in length, pre-stressed UHPC I-girder and four different UHPC 2nd generation pi-girders. The length of I-girders is 24.4 m, 7.3 m and 9.2 m, respectively. The 2nd generation pi-girder length is 7.6 m [29]. Based on the linear complementary problem (LCP), Guo et al investigated the applicability of numerical simulation to predict the failure surface of three different UHPC-I girders and validate results by comparing experimental results and finite element analysis of DIANA software. The fracture result comparison between the LCP method and the experimental result shows a similar tendency, implying that the LCP model can capture the behavior of the UHPC girder before and after peak load [26]. According to the literature survey, more experiments and finite element studies are needed on large-scale UHPC pre-stressed girders.

Table 1. Advantages and disadvantages of some kind of box girder.

Case	Advantage	Disadvantage
Pre-stressed Concrete Box Girder	Reduces the thickness of deck and self-weight of structure	High cost of logistic and transportation
	Higher strength per unit concrete area	High deflection at the mid-span after a period of operation
	Quality assurance with precast segments	Crack in long-span after a period of operation
	Reasonable cost	
Steel Composite Box Girder	Greater aerodynamic stability	Greater fabrication cost due to reduced scope for automated fabrication
	Support point required are less compared to conventional systems	Steel girders are costly
	Provide better appearance and slender shape	High maintenance cost, not suitable for aggressive environment
Pre-stressed UHPC Box Girder	All advantages of Pre-stressed Concrete Box Girder	
	Higher torsional stiffness than steel composite girder	Logistical inefficiencies and transportation cost
	Shaping is flexible	Require advanced production technology
	Suitable design in highly aggressive environments	
	Total lower cost	

Table 1 shows the advantages and disadvantages of UHPC box girder compared to other girders. While UHPC has been under research and development for over thirty years, it is still a relatively new material. The lack of understanding on structural behavior of UHPC elements are some of the major factors in slowing the implementation of this technology.

The objective of the paper is to investigate the flexural behavior of UHPC box girder strengthened with pre-stressed tendons. A 3D simulation model of the 60 m UHPC pre-stressed box girder, using concrete damage plasticity (CDP) approach, was implemented. Furthermore, the well-fitted constitutive models both compressive and tensile nonlinear behavior of the material, which plays an important part of numerical simulation, will be conducted in this study.

2. Methods

In terms of the existing constitutive model, the Concrete Damage Plasticity (CDP) which is based on continuum, plasticity, and damaged state for concrete, and has been implemented in ABAQUS for numerical simulation. CDP model was firstly introduced by Lubliner et al. for monotonic loading [33]. Due to the advantages of the CDP model to capture the behavior of concrete materials, in the present study, the concrete damage plasticity (CDP) model is chosen to investigate the flexural behavior of the UHPC box girder. Fig. 1 depicts tension behavior and compressive behavior in the CDP model. In the CDP

model, the uniaxial tension stress-strain relation is assumed linearly elastic until failure stress of f_t^0. For uniaxial compression, the response is linear up to the initial yield f_c^0.

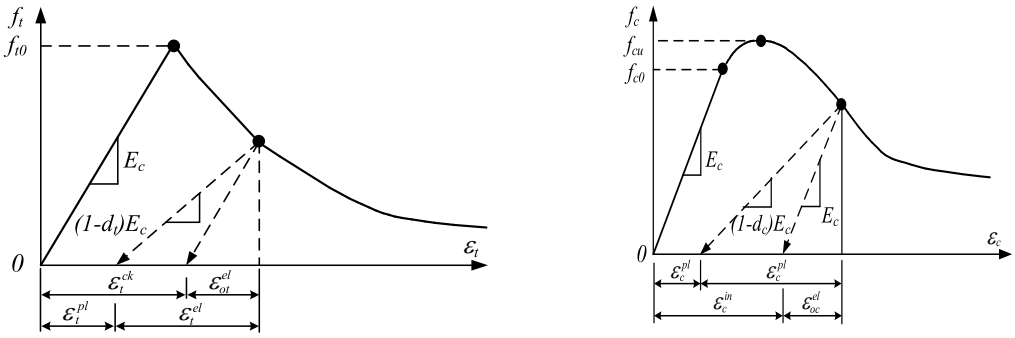

a) **b)**

Figure 1. Tension behavior (a) and Compressive behavior in the CDP model (b).

After reaching the ultimate stress in the plastic zone, the response of concrete is described by the stress hardening followed by strain softening. Stresses of the concrete element f_t and f_c determined to unload from any point on the strain are:

$$f_t = E_c\left(\varepsilon_t - \varepsilon_t^{pl}\right)\left(1-d_t\right), \tag{1}$$

$$f_c = E_c\left(\varepsilon_c - \varepsilon_c^{pl}\right)\left(1-d_c\right), \tag{2}$$

where E_c denotes Young's modulus of concrete. ε_t, ε_c are the strain in tension and compression. ε_t^{pl}, ε_c^{pl} define the plastic strain in tension and compression. Damage variables d_t and d_c define the degradation of the elastic stiffness. To determine the failure surface, the effective tensile $\overline{f}_t$ and compressive cohesion stresses $\overline{f}_c$ of concrete can be calculated by:

$$\overline{f}_t = \frac{f_t}{1-d_t} = E_c\left(\varepsilon_t - \varepsilon_t^{pl}\right), \tag{3}$$

$$\overline{f}_c = \frac{f_c}{1-d_c} = E_c\left(\varepsilon_c - \varepsilon_c^{pl}\right). \tag{4}$$

The relationship of the cracking strain and plastic strain can be expressed by:

$$\varepsilon_t^{pl} = \varepsilon_t^{ck} - \frac{d_t}{1-d_t}\frac{f_t}{E_0}, \tag{5}$$

$$\varepsilon_c^{pl} = \varepsilon_c^{ck} - \frac{d_c}{1-d_c}\frac{f_c}{E_0}, \tag{6}$$

where ε_t^{ck}, ε_c^{ck} present the cracking strain, which can be obtained by the total strain minus the elastic strain corresponding to the undamaged material.

3. Results and Discussion

3.1. Validation of simulation model

This section includes the validation of the FE model in Abaqus using the CDP approach to ensure that the proposed model has been correctly implemented and is thereby further used to investigate the flexural behavior of UHPC pre-stressed box girder. The proposed model is verified by comparing the results with the tests of the UHPC beam conducted by Yang et al. Fig. 2 shows the constitutive law of UHPC material in compression and tension behaviour [34]. Input parameters of the CDP model for UHPC material are presented in Table 2.

In the test of Yang, the length of the UHPC beam is 2900 mm with the dimension of cross-section 180 mm × 270 mm, is shown in Fig. 3. The NR1 beam denotes the UHPC plain specimen without the steel bar, whereas the R13 beam includes three steel bars with 13 mm diameter corresponding to the steel bar ratio of 0.9 %, using class of SD400 in Korean code. Fig. 4. shows the test setup of Yang for NR1 beam and R13 under four-point bending moment test.

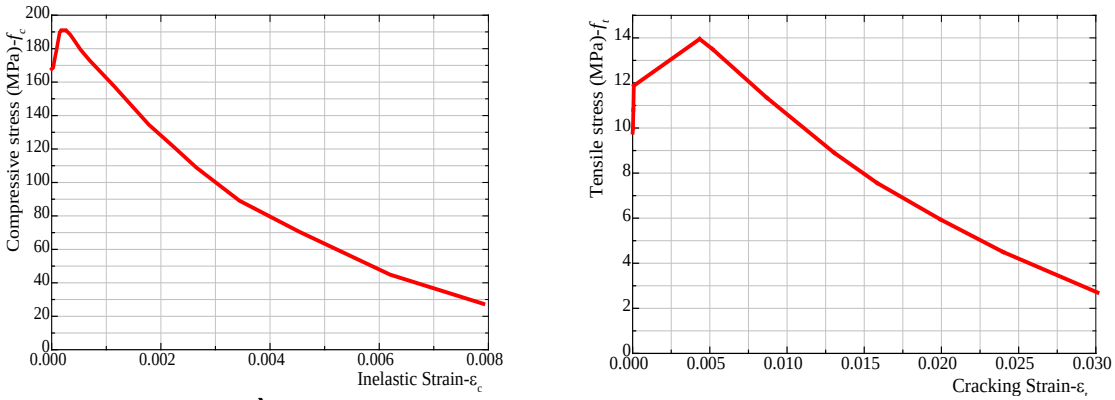

Figure 2. Compressive stress – inelastic strain (a), and Tensile stress – cracking strain of UHPC.

Table 2. Input parameters of CDP model for UHPC.

Property	UHPC
Mass density (ton/mm^3)	2.45e^{-9}
Compressive strength (MPa)	190.9
Modulus of elasticity (MPa)	46418
Poisson's ratio	0.2
Dilation angle ψ (^{0})	36
Eccentricity ϵ	0.1
Stress ratio σ_{bo}/σ_{co}	1.16
Shape parameter (K_c)	0.667
Viscosity parameter μ	0

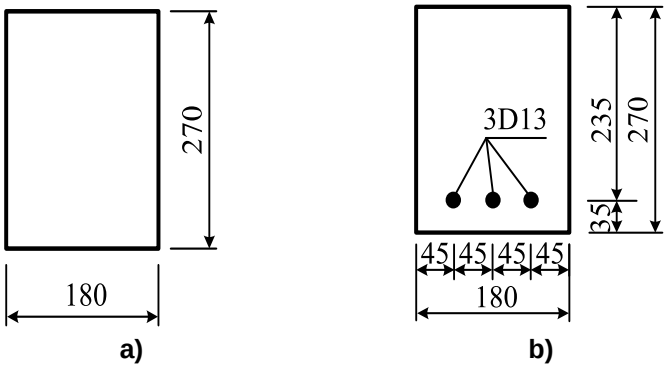

Figure 3. Cross section of Beam NR1 (a), and R13 (b) (mm).

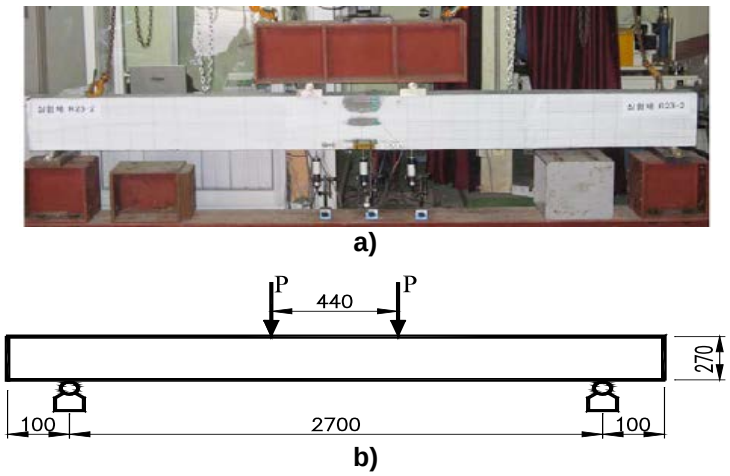

Figure 4. Test setup of Yang.

Load-deflection curves in the test of Yang and simulation are shown in Fig. 5. The peak load and maximum deflection of beam NR1 and R13 according to the test of Yang and simulation result are listed in Table 3. The load-deflection curve obtained by the proposed model is generally similar to the test data, however, the maximum deflection response exhibits the disparity in both cases. The load-deflection curve in the simulation result shows stiffer behavior than the corresponding results from the test. The development of microcracks due to dry shrinkage, UHPC material curing, experimental process, and so on, could be the reason for this disparity. In addition, in the Abaqus model, the concrete–steel interaction is assumed as embedded interaction, implying an idealization interaction. This perfect interaction can also contribute to the superior stiffness in the numerical model.

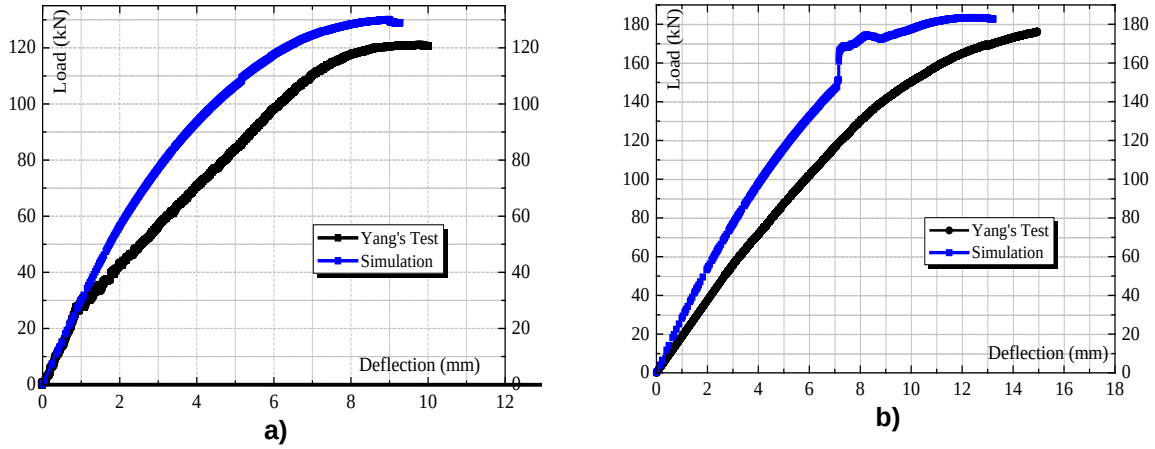

Figure 5. Load-deflection curve in the test of Yang and simulation for beam NR1 (a) and R13(b).

Table 3. Peak load and maximum deflection of beam NR1 and R13.

Beam	Peak load (1)	Peak load (2)	Disparity	Max. deflection (1)	Max. deflection (2)	Disparity
NR1	120.2 kN	128.8 kN	7.2 %	10.3 mm	9.2 mm	13.1 %
R13	174.6 kN	183.7 kN	5.1 %	15.1 mm	12.8 mm	15.2 %

Note: (1) – Yang's test; (2) – Simulation's result

The crack pattern observed in the simulation model is quite similar to the test of Yang, are shown in Fig. 6. Initial, first cracks occurred at flexural zones under loading points. Later on, following the increase of applied load, newer cracks evolved as older cracks propagated wider and deeper in the flexural and shear zone. It can be seen that the CDP model and the constitutive law of material demonstrated the accuracy of the simulation of the UHPC girder under the four-point bending test. Based on the obtained result, the proposed model will be developed to investigate the flexural behavior of 60 UHPC box girder.

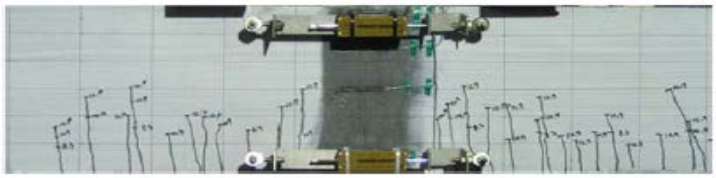

a)

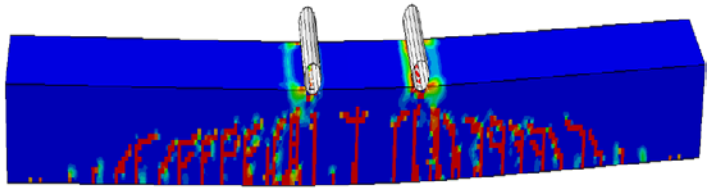

b)

Figure 6. Crack pattern in the test of Yang (a) and simulation (b).

3.2. Finite element model development for 60 m UHPC box-girder

3.2.1. Description of 60 m UHPC box girder

Detail of the UHPC box girder adapted from the first project of the high-speed train in Vietnam. Fig. 7 shows the plan and front view of the UHPC box girder. The cross-section of the girder consists of a UHPC U-shaped part, UHPC deck plate (50 mm), and high strength concrete (HSC) reinforced plate (200 mm) with compressive strength of 40 MPa. The width of the box girder changes from 1600 mm to 2600 mm corresponding to the bottom surface and upper surface. The UHPC box girder contains 2×8 pre-stressed tendons in the upper flange and 6×24 pre-stressed tendons in the lower flange. The 50 mm UHPC plate without reinforcement bar and 200 mm HSC plate with two layers of steel bar are shown in Fig. 8. Parameters of the pre-stressed tendon are taken according to Vietnamese standard and shown in Table 4, in which a tendon cluster is applied a force equivalent to 4853 kN [35].

Table 4. Pre-stressed load of tendon.

Strand	Total area (mm^2)	Ultimate stress fy (MPa)	Pre-stressed Force 0.7 fy (MPa)
24	3328.8	2100	1470

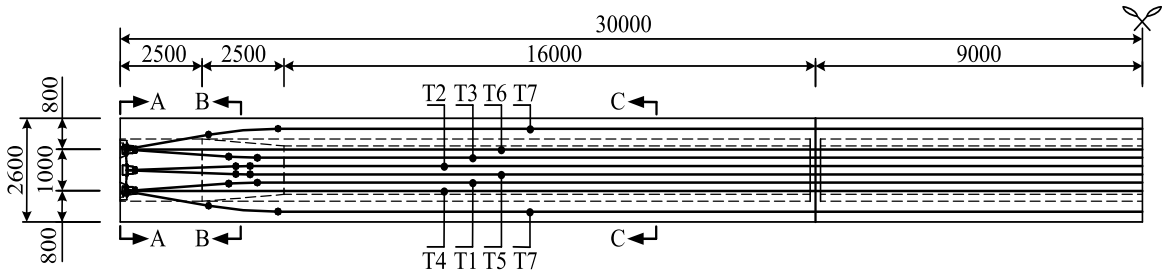

a)

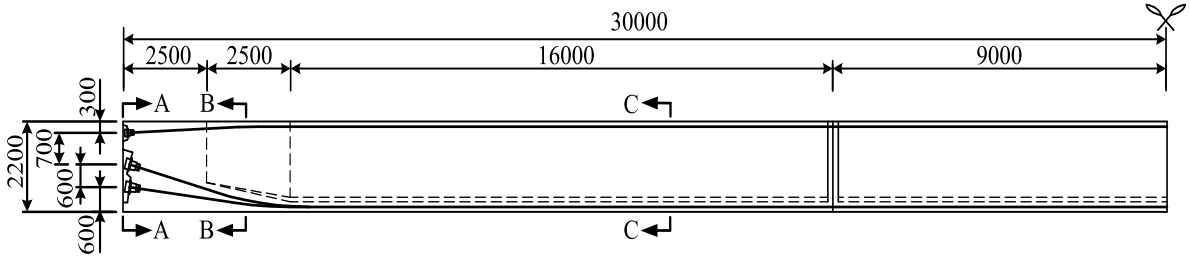

b)

Figure 7. Plan (a) and front view (b) of UHPC box girder (mm).

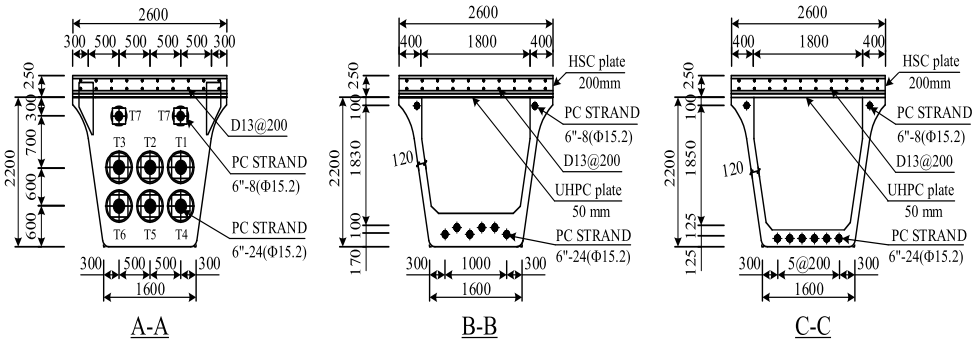

Figure 8. Cross sections of UHPC box girder.

3.2.2. Numerical Results

The input parameters for the UHPC material are adopted as the proposed model. In the Abaqus model, C3D8R and T3D2 element types are selected to simulate concrete and longitudinal bar. C3D8R element (Fig. 9) is defined as a continuum element with reduced integration and hourglass control, which can describe concrete cracking in tension and crushing in compression. T3D2 presents a two-node, three-dimensional truss element used to simulate slender and line elements. There is no moment or perpendicular force to the centerline of this element. The interaction of the UHPC-HSC plate is a tie connection while the embedded property is applied for the interaction of concrete-tendon and concrete-steel bar. The constitutive model of UHPC includes compression post-peak, tension-softening behavior is described by the stress-strain curve in the CDP model (Fig. 2). The box girder is supported by two simple rollers for each end. Three types of loads are applied including self-weight, post-tensioning, and displacement load. In the FE model, self-weight is calculated as a gravity load. To obtain the nonlinear behavior of the box girder, displacement is adopted instead of concentrated load. A pair of –80 mm displacement is applied on the top surface of the HSC plate. Fig. 10 shows the full 3D model of the UHPC box girder.

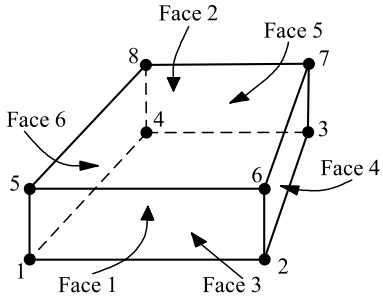

Figure 9. C3D8R element type in Abaqus modeling.

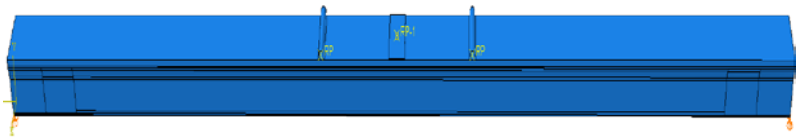

Figure 10. Full 3D model of UHPC box girder under four-point bending test Load-deflection curve.

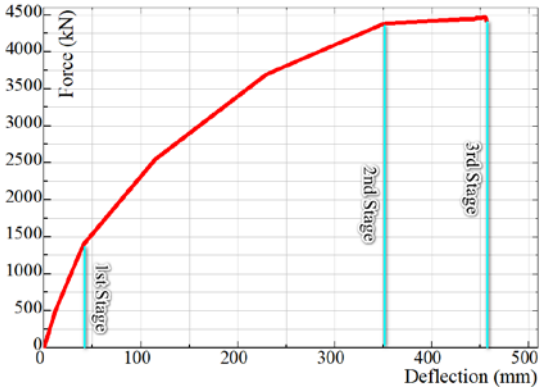

Figure 11. P-U curve of UHPC box girder.

The load-displacement curve of the UHPC box girder is depicted in Fig. 11. The load-displacement curve shows three stages. The first stage is from the beginning of the simulation process to the load of 1325.6 kN, which is nearly 29 % of the peak load (4475.2 kN). At this stage, the load-displacement curve exhibits elastic behavior. The initial crack occurs at the load of 1325.6 kN, corresponding to the deflection of 48.2 mm at the midspan. At the second stage, the applied load is observed from 1325.6 kN to 4390.4 kN, strain-hardening appeared and propagated along the surface of the box girder, concentrated under loading point and midspan. Unlike the first stage, at the second stage, the load-displacement curve shows the nonlinear behavior with the multiple crack propagation. At the load of 4390.4 kN, the observed deflection value is 350.3 mm. At the third stage, loading from 4390.4 kN reaches the maximum value of 4475.8 kN with a deflection of 455.9 mm. The P-U curve shows plasticity behavior, where load increment is considerably smaller than the previous stage. The peak load is observed in this stage at 4475.8 kN. After this moment, the P-U curve starts to the downward nonlinear trend.

Fig. 12 shows the Von-mises contour stress of the box girder. Under peak load of 4475.8 kN, the stress in the HSC plate reaches the ultimate limit of compressive strength, resulting in crushing failure, whereas the UHPC girder exhibits strain softening behavior in the tensile region. These results would seem to suggest that in order to obtain full capacity of UHPC material, the higher compressive strength of HSC material is necessary.

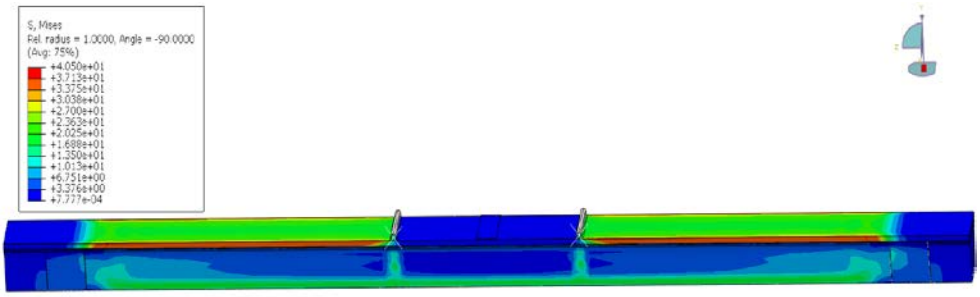

Figure 12. Stress contour in the box girder.

Strain profile

In order to measure the longitudinal strain of the UHPC box girder, the elements are extracted from the simulation model at mid span and joint sections in Fig. 13. Fig. 14a shows the strain profile of the UHPC box girder at mid-span. The initial yielding strain occurs at 1325.6 kN, in which strain values are –150.2 με in compression at HSC slab (S5), –105.8 με in compression at UHPC slab (S4), and 207.2 με in tension at the bottom of the UHPC girder (S1), respectively. At load level of 4390 kN, HSC slab exhibits inelastic, strain hardening behavior in compression with strain value of –2507.3 με, while UHPC plate is under elastic behavior in compression with strain value of –1860.1 με. UHPC box girder has a strain value of 5507.3 με in tension. At the peak load of 4475 kN, FE analysis predicts the strain values of elements increase rapidly. The HSC plate (S5) undergoes inelastic, strain hardening behavior in compression with the strain values of –2817.2 με, whereas the UHPC plate (S4) shows linear elastic behavior in compression with strain values of –2019.8 με. UHPC box girder exhibits the strain-softening behavior in the tension of 7913.8 με.

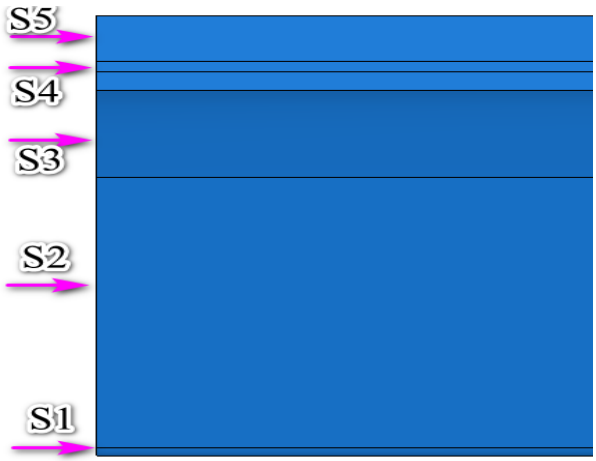

Figure 13. Position to take strain data from FE model.

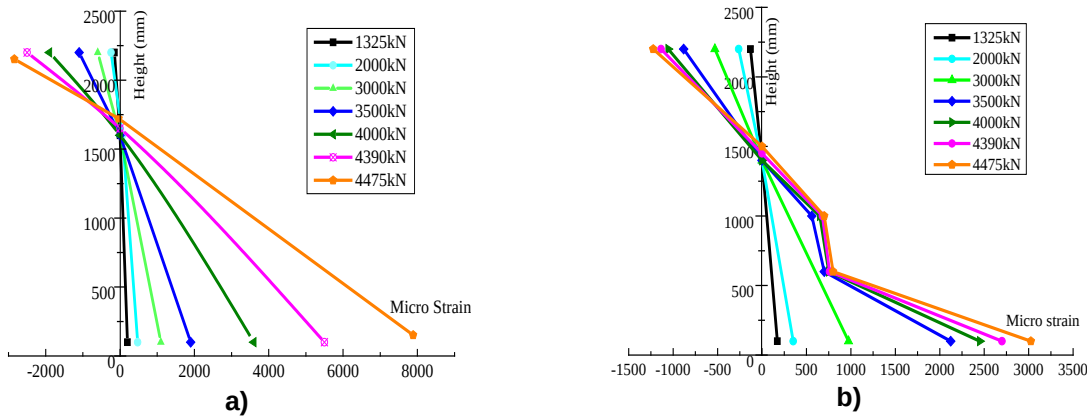

Figure 14. Longitudinal strain profile at mid span (a) and joint section (b).

Strain at the joint section shows a similar trend to what has been reported at the mid-span of the box girder. However, strain at the joint section has a significantly smaller value than in the mid-span (Fig. 14b). For instance, at the maximum load of 4475.8 kN, HSC (S5) and UHPC (S4) slab exhibit linear elastic behavior with strain value of –1224.5 με and –920.8 με in compression, respectively. Meanwhile, the UHPC girder (S1) shows strain-hardening behavior with a strain value of 3024.4 με. The curvature difference of strain at joint section in Fig. 14b appears due to the discrete crack as increasing of applied load.

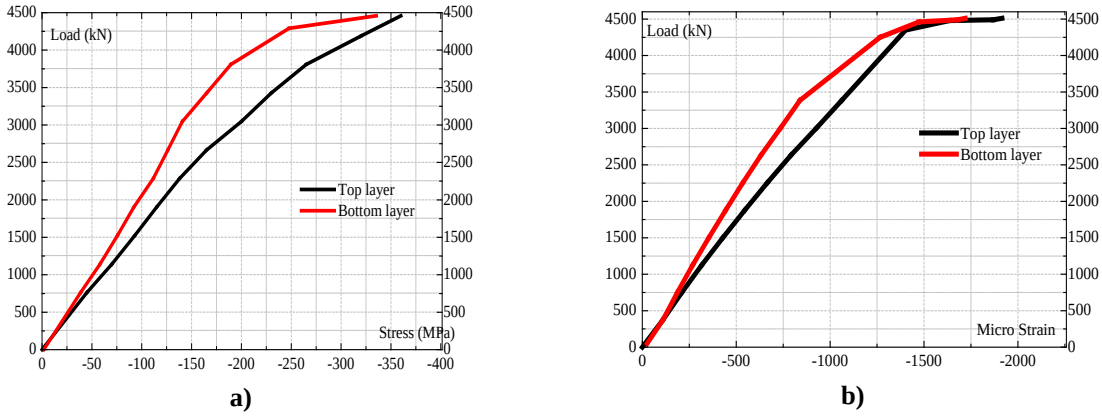

Figure 15. Stress (a) and strain (b) versus load in longitudinal steel bars at mid span.

Fig. 15 depicts the stress and strain versus load in longitudinal steel bar of HSC plate. At the moment of first cracks appearance with the load of 1325.6 kN, stress and strain of longitudinal bar in the bottom layer is –67.9 MPa and –286.1 με, respectively. Stress and strain of longitudinal bar in the top layer are –78.3 MPa and –364.8 με. Both layers of longitudinal steel bar exhibit elastic behavior. Under the maximum load of 4475.8 kN, stress and strain in the bottom layer reach the value of –340.8 MPa and –1741.7 με, while in the top layer are –362.4 MPa and –1915.8 με. The top and bottom longitudinal steel bars show perfect plastic behavior.

Fig. 16 depicts stress and strain versus the vertical load of tendons at mid-span. Compared to lower tendons, upper tendons have smaller stress and strain. The maximum value of stress and strain in the upper tendons is 853.7 MPa and 3240.7 με, respectively. Upper tendons exhibit linear elastic behavior. On the contrary, the lower tendons show larger stress and strain than the upper tendons. The stress-strain curve consists of two stages. In the first stage from beginning to the load of 1325.6 kN, stress-strain values are 1136.4 MPa and 6283.5 με. The tendons show elastic behavior. Following the increment in applied load, there is a tremendous increase of stress and strain in lower tendons. At the peak load of 4476 kN, stress and strain reach the value of 1428.2 MPa and 12864.1 με, respectively. The lower tendons show plastic behavior.

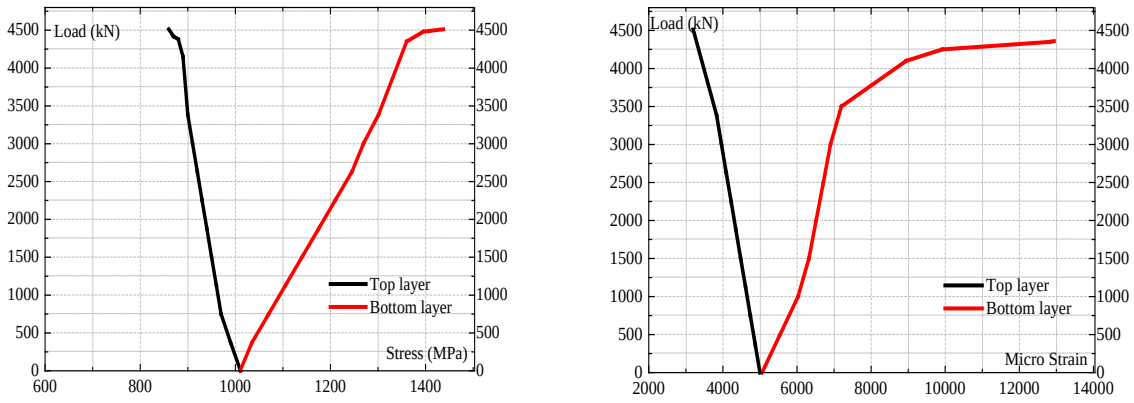

a) b)

Figure 16. Stress (a) and strain (b) versus load in tendons at mid span Cracking Pattern.

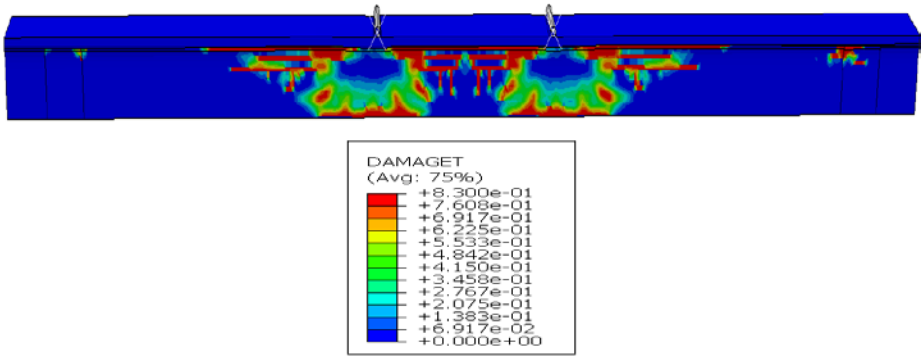

Figure 17. Crack pattern in the box girder.

Fig. 17 shows the cracking pattern of the box girder versus increasing the load. The first cracks occurred at a load of 1325.6 kN. During the increment of the vertical load until the maximum value, the crack pattern propagates rapidly along the longitudinal axis of the box girder. At the load level of 1325.6 kN, cracks are distributed along 10.2 m length at mid-span. At the peak load of 4475.8 kN, the length of the crack distribution is 15.8 m.

4. Conclusions

The study presents the structural behavior of the pre-stressed UHPC box girder. Using the CDP model, the numerical simulation determined the appropriate constitutive model in the compressive and tensile behavior of the UHPC box girder. The proposed model was proved with experimental results of the short span UHPC beam under the four-point bending moment test. Later on the model was developed to simulate 60 m pre-stressed UHPC box girder. The following conclusions are drawn:

1. The prediction of flexural behavior of the UHPC box girder shows three different stages of box girder, including: From the first point to the occurrence of initial crack, corresponding to the elastic phase of material; The initial crack to the propagation of multiple cracks, which describe the nonlinear behavior; The stage of plasticity behavior and finally downward nonlinear behavior results in failure of the girder.

2. At the maximum value of the applied load, the top and bottom longitudinal steel bars in the HSC plate show perfect plastic behavior. The prestressed tendons exhibit different behaviors depending on the location. Under applied load, the upper tendons undergo compressive stress with linear elastic behavior. In contrast to upper tendons, lower tendons are in tension stress and show plasticity behavior under maximum load.

3. First cracks occur perpendicularly to the bottom edge of the box girder at mid-span. The increment in vertical load leads to rapid formation and propagation of perpendicular and diagonal cracks along the longitudinal axis of the girder. Based on the obtained result, while the HSC plate shows failure under maximum load, stresses in UHPC girder is significantly smaller than ultimate strength. In order to utilize full capacity of UHPC material, the strength of conventional concrete in the box girder should be improved.

References

1. Wang, J.Y., Bian, C., Xiao, R.C., Ma, B. Restrained Shrinkage Mechanism of Ultra High Performance Concrete. KSCE Journal of Civil Engineering. 2019. 23(10). Pp. 4481–4492. DOI: 10.1007/s12205-019-0387-5
2. Arora, A., Aguayo, M., Hansen, H., Castro, C., Federspiel, E., Mobasher, B., Neithalath, N. Microstructural packing- and rheology-based binder selection and characterization for Ultra-high Performance Concrete (UHPC). Cement and Concrete Research. 2018. 103(February). Pp. 179–190. DOI: 10.1016/j.cemconres.2017.10.013. URL: http://dx.doi.org/10.1016/j.cemconres.2017.10.013
3. Le Hoang, A., Fehling, E. Influence of steel fiber content and aspect ratio on the uniaxial tensile and compressive behavior of ultra high performance concrete. Construction and Building Materials. 2017. 153(November). Pp. 790–806. DOI: 10.1016/j.conbuildmat.2017.07.130. URL: http://dx.doi.org/10.1016/j.conbuildmat.2017.07.130
4. Tian, H., Zhou, Z., Zhang, Y., Wei, Y. Axial behavior of reinforced concrete column with ultra-high performance concrete stay-in-place formwork. Engineering Structures. 2020. 210(February). Pp. 110403. DOI: 10.1016/j.engstruct.2020.110403. URL: https://doi.org/10.1016/j.engstruct.2020.110403
5. Yujing, L., Wenhua, Z., Fan, W., Peipei, W., Weizhao, Z., Fenghao, Y. Static mechanical properties and mechanism of C200 ultra-high performance concrete (UHPC) containing coarse aggregates. Science and Engineering of Composite Materials. 2020. 27(1). Pp. 186–195. DOI: 10.1515/secm-2020-0018
6. He, S., Deng, Z. Seismic Behavior of Ultra-High Performance Concrete Short Columns Confined with High-Strength Reinforcement. KSCE Journal of Civil Engineering. 2019. 23. Pp. 5183–5193. DOI: 10.1007/s12205-019-0915-3
7. Mao, L., Barnett, S.J. Investigation of toughness of ultra high performance fibre reinforced concrete (UHPFRC) beam under impact loading. International Journal of Impact Engineering. 2017. 99. Pp. 26–38. DOI: 10.1016/j.ijimpeng.2016.09.014. URL: http://dx.doi.org/10.1016/j.ijimpeng.2016.09.014
8. Meng, W., Valipour, M., Khayat, K.H. Optimization and performance of cost-effective ultra-high performance concrete. Materials and Structures/Materiaux et Constructions. 2017. 50(1). DOI: 10.1617/s11527-016-0896-3
9. Yoo, D.Y., Banthia, N. Mechanical properties of ultra-high-performance fiber-reinforced concrete: A review. Cement and Concrete Composites. 2016. 73. Pp. 267–280. DOI: 10.1016/j.cemconcomp.2016.08.001. URL: http://dx.doi.org/10.1016/j.cemconcomp.2016.08.001
10. Wu, Z., Shi, C., He, W., Wang, D. Static and dynamic compressive properties of ultra-high performance concrete (UHPC) with hybrid steel fiber reinforcements. Cement and Concrete Composites. 2017. 79. Pp. 148–157. DOI: 10.1016/j.cemconcomp.2017.02.010. URL: http://dx.doi.org/10.1016/j.cemconcomp.2017.02.010
11. Hosinieh, M.M., Aoude, H., Cook, W.D., Mitchell, D. Behavior of ultra-high performance fiber reinforced concrete columns under pure axial loading. Engineering Structures. 2015. 99. Pp. 388–401. DOI: 10.1016/j.engstruct.2015.05.009. URL: http://dx.doi.org/10.1016/j.engstruct.2015.05.009
12. Qian, D., Yu, R., Shui, Z., Sun, Y., Jiang, C., Zhou, F., Ding, M., Tong, X., He, Y. A novel development of green ultra-high performance concrete (UHPC) based on appropriate application of recycled cementitious material. Journal of Cleaner Production. 2020. 261. Pp. 121231. DOI: 10.1016/j.jclepro.2020.121231. URL: https://doi.org/10.1016/j.jclepro.2020.121231
13. Graybeal, B. UHPC in the US Highway Infrastructure. Designing and Building with UHPFRC. 2013. (November 2009). Pp. 221–234. DOI: 10.1002/9781118557839.ch15
14. Schmidt, M., Leutbecher, T., Piotrowski, S., Wiens, U. The German Guideline for Ultra-High Performance. UHPFRC 2017 Designing and Building with UHPFRC: New large-scale implementations, recent technical advances, experience and standards. 2017. 2(1). Pp. 545–554.
15. Toutlemonde, F., Bernardi, S., Brugeaud, Y., Simon, A. Twenty years-long French experience in UHPFRC application and paths opened from the completion of the standards for UHPFRC. 2018. URL: https://hal.archives-ouvertes.fr/hal-01955204
16. Toutlemonde, F., Généreux, G., Delort, M., Resplendino, J. Product and Design Standards for UHPFRC in France. 2016. (January). DOI: 10.21838/uhpc.2016.114
17. Schmidt, M., Fehling, E. Ultra-high-performance concrete: Research, development and application in Europe. Seventh International Symposium on the Utilization of High Strength/High-Performance Concrete. 2005. (September 2015). Pp. 51–78. URL: http://download.contec-aps.com/uploads/tx_mpdownloadcenter/pp_fp_2005_003_eng_01.pdf
18. Graybeal, B.A. Compressive Behavior of Ultra-High-Performance Fiber-Reinforced Concrete. ACI Materials Journal. 2007. 104. Pp. 46–152.
19. Freytag, B., Heinzle, G., Reichel, M., Sparowitz, L. WILD- Bridge scientific preparation for smooth realisation. Proceeding of 3rd International Symposium on UHPC and Nanotechnology for High Performance Construction Materials. 2012. Pp. 881–888.
20. Rebentrost, M., Wight, G. Perspective on UHPCs from a specialist construction Company. ISTE, London, 2011. Pp. 189–206.
21. Rebentrost, M., Wight, G., Fehling, E. Experience and Applications of Ultra-high Performance Concrete in Asia. 2nd International Symposium on Ultra High Performance Concrete. 2008. Pp. 19–30.
22. Kim, B.-S., Joh, C., Park, S.Y., Koh, G.-T., Kwon, K., Park, J. KICT's Application of UHPC to the First UHPC Cable Stayed Roadway Bridge. 2016. Pp. 1–9. DOI: 10.21838/uhpc.2016.97
23. Lee, C., Kim, K., Choi, S. Application of Ultra high performance concrete to pedestrian cable-stayed bridges. Journal of Engineering Science and Technology. 2013. 8(3). Pp. 296–305.
24. Tanaka, Y., Maekawa, K., Kameyama, Y., Ohtake, A., Musha, H., Watanabe, N. The Innovation and Application of UHPFRC Bridges in Japan. Designing and Building with UHPFRC. 2013. (October). Pp. 149–188. DOI: 10.1002/9781118557839.ch12
25. Voo, Y.L., Foster, S., Pek, L.G. Ultra-high performance concrete – Technology for present and future 2017.
26. Guo, Q., Han, S.-M. Flexural Behavior of Ultra High Performance Fiber Reinforced Concrete Segmental Box Girder. Journal of the Korea Concrete Institute. 2014. 26(2). Pp. 109–116. DOI: 10.4334/jkci.2014.26.2.109
27. Yang, I.H., Joh, C., Kim, B.S. Flexural strength of large-scale ultra high performance concrete prestressed T-beams. Canadian Journal of Civil Engineering. 2011. 38(11). Pp. 1185–1195. DOI: 10.1139/l11-078
28. Guo, Q., Han, S.-M. Flexural Behavior of Ultra High Performance Fiber Reinforced Concrete Segmental Box Girder. Journal of the Korea Concrete Institute. 2014. 26. DOI: 10.4334/JKCI.2014.26.2.109
29. Chen, L., Graybeal, A.B. Finite element analysis of ultra-high performance concrete: Modeling structural performance of an AASHTO type II girder and a 2nd generation pi-girder 2010.

30. Singh, M., Sheikh, A.H., Mohamed Ali, M.S., Visintin, P., Griffith, M.C. Experimental and numerical study of the flexural behaviour of ultra-high performance fibre reinforced concrete beams. Construction and Building Materials. 2017. 138. Pp. 12–25. DOI: https://doi.org/10.1016/j.conbuildmat.2017.02.002. URL: https://www.sciencedirect.com/science/article/pii/S0950061817301770
31. Behloul, M., Lee, K.C. Seonyu footbridge. Structural Concrete. 2003. 4. Pp. 195–201.
32. Lafarge. Ductal® – Applications and References. 2020URL: http://www.ductal-lafarge.com/wps/portal/Ductal/Applications-AndReferences/
33. Lubliner, J., Oliver, J., Oller, S., Onate, E. a Plastic-Damage Model. International Journal of Solids and Structures. 1989. 25(3). Pp. 299–326.
34. Yang, I.H., Joh, C., Kim, B.S. Structural behavior of ultra high performance concrete beams subjected to bending. Engineering Structures. 2010. 32(11). Pp. 3478–3487. DOI: 10.1016/j.engstruct.2010.07.017. URL: http://dx.doi.org/10.1016/j.engstruct.2010.07.017.
35. Vietnamese Ministry of Construction, V.M. of C. Precast Prestressed concrete product – Technical requirements and acceptance test2014. 1–86 p.

Information about authors:

Van Tu Nguyen
ORCID: https://orcid.org/0000-0002-0298-5080
E-mail: nguyentu@lqdtu.edu.vn

Viet Chinh Mai, PhD
ORCID: https://orcid.org/0000-0002-2285-3034
E-mail: maivietchinh@lqdtu.edu.vn

Received 26.02.2021. Approved after reviewing 23.08.2021. Accepted 23.08.2021.